A&A 612, L10 (2018)
https://doi.org/10.1051/0004-6361/201833074

Astronomy & Astrophysics

LETTER TO THE EDITOR

Discovery of the elusive radical NCO and confirmation of H_2NCO^+ in space⋆

N. Marcelino[1], M. Agúndez[1], J. Cernicharo[1], E. Roueff[2], and M. Tafalla[3]

[1] Instituto de Física Fundamental, CSIC, C/ Serrano 123, 28006 Madrid, Spain
[2] Sorbonne Université, Observatoire de Paris, Université PSL, CNRS, LERMA, 92190 Meudon, France
[3] Observatorio Astronómico Nacional (OAN), C/ Alfonso XII 3, 28014 Madrid, Spain

Received 22 March 2018 / Accepted 11 April 2018

ABSTRACT

The isocyanate radical (NCO) is the simplest molecule containing the backbone of the peptide bond, C(=O)–N. This bond has a prebiotic interest since it links two amino acids to form large chains of proteins. It is also present in some organic molecules observed in space such as HNCO, NH_2CHO, and CH_3NCO. In this letter, we report the first detection in space of NCO towards the dense core L483. We also report the identification of the ion H_2NCO^+, which definitively confirms its presence in space, and observations of HNCO, HOCN, and HCNO in the same source. For NCO, we derive a column density of 2.2×10^{12} cm^{-2}, which means that it is only ∼5 times less abundant than HNCO. We find that H_2NCO^+, HOCN, and HCNO have abundances relative to HNCO of 1/400, 1/80, and 1/160, respectively. Both NCO and H_2NCO^+ are involved in the production of HNCO and several of its isomers. We have updated our previous chemical models involving NCO and the production of the CHNO isomers. Taking into account the uncertainties in the model, the observed abundances are reproduced relatively well. Indeed, the detection of NCO and H_2NCO^+ in L483 supports the chemical pathways to the formation of the detected CHNO isomers. Sensitive observations of NCO in sources in which other molecules containing the C(=O)–N subunit have been detected could help elucidate its role in prebiotic chemistry in space.

Key words. astrochemistry – ISM: clouds – ISM: abundances – stars: formation – stars: low-mass – line: identification

1. Introduction

Most molecules observed in space can be formed with just the four atoms H, C, N, and O. These atoms are the building blocks of organic and prebiotic molecules, and arranged together, constitute the backbone of the peptide bond R–C(=O)–N(–H)–R′, which links two amino acids and allows the building of large proteins. Therefore, the observation of simple molecules with the C(=O)–N group in space can provide important clues on the earliest chemical steps in the synthesis of amino acids. The isocyanate radical (NCO) is the simplest such species and it is predicted to be abundant in dark clouds (Prasad & Huntress 1978; Marcelino et al. 2009). It is also the main precursor of isocyanic acid (HNCO), a species that has been found in a large variety of interstellar environments (see Marcelino et al. 2009, and references within).

HNCO has several metastable isomers: HOCN, HCNO, and HONC, which lie at 24.7, 70.7, and 84.1 kcal mol^{-1} with respect to HNCO (see Schuurman et al. 2004). Two of these isomers, HCNO and HOCN, have also been previously detected in molecular clouds (Marcelino et al. 2009; Marcelino et al. 2010; Brünken et al. 2010). The chemical pathways to the formation of these species are diverse, but the main precursors in the gas phase are the radicals NCO and CNO (Marcelino et al. 2010; Quan et al. 2010). Following protonation and hydrogenation, these radicals lead to the protonated CHNO ions H_2NCO^+, $HNCOH^+$, $HCNOH^+$, H_2OCN^+, and H_2CNO^+ (Marcelino et al. 2010; Quan et al. 2010). By dissociative recombination (DR) reactions, these ions could produce all the CHNO isomers, including the highest isomer in energy HONC not detected so far in space and also the NCO radical (Marcelino et al. 2010). The two isomeric forms of the protonated isocyanic acid H_2NCO^+ and $HNCOH^+$ have been studied in the laboratory (Lattanzi et al. 2012; Gupta et al. 2013), and H_2NCO^+ has been tentatively detected in absorption of the low-lying rotational transitions in the centimetre band towards the molecular cloud Sgr B2(N) by Gupta et al. (2013).

In this letter, we report the first detection in space of NCO and we confirm the presence of H_2NCO^+ through millimetre emission transitions. These species were detected towards L483, a dense core located in the Aquila Rift, which hosts the protostar IRAS 18148−0440 that is in transition from Class 0 to Class I and which shows infall motions and a collimated molecular outflow (Tafalla et al. 2000; Park et al. 2000). Based on the bright emission of carbon chains such as C_4H (Agúndez et al. 2008; Sakai et al. 2009), it has been suggested that L483 may host a warm carbon-chain chemistry environment. Apart from carbon chains, L483 is also rich in O-bearing organic molecules such as HCO, HCCO, H_2CCO, CH_3CHO, HCCCHO, and c-C_3H_2O (Agúndez et al. 2015a; Loison et al. 2016). Recently, the chemical richness of the source has been evidenced with the discovery of several new molecules: HCCO, $NCCNH^+$, NS^+, HCS, and HSC (Agúndez et al. 2015a,b, 2018; Cernicharo et al. 2018). Recent ALMA observations have shown a chemical differentiation in L483, which has carbon chains such as C_2H tracing the envelope and more complex organics such as HNCO, NH_2CHO, and $HCOOCH_3$ distributed around the protostar (Oya et al. 2017).

⋆ Based on observations carried out with the IRAM 30 m telescope. IRAM is supported by INSU/CNRS (France), MPG (Germany), and IGN (Spain).

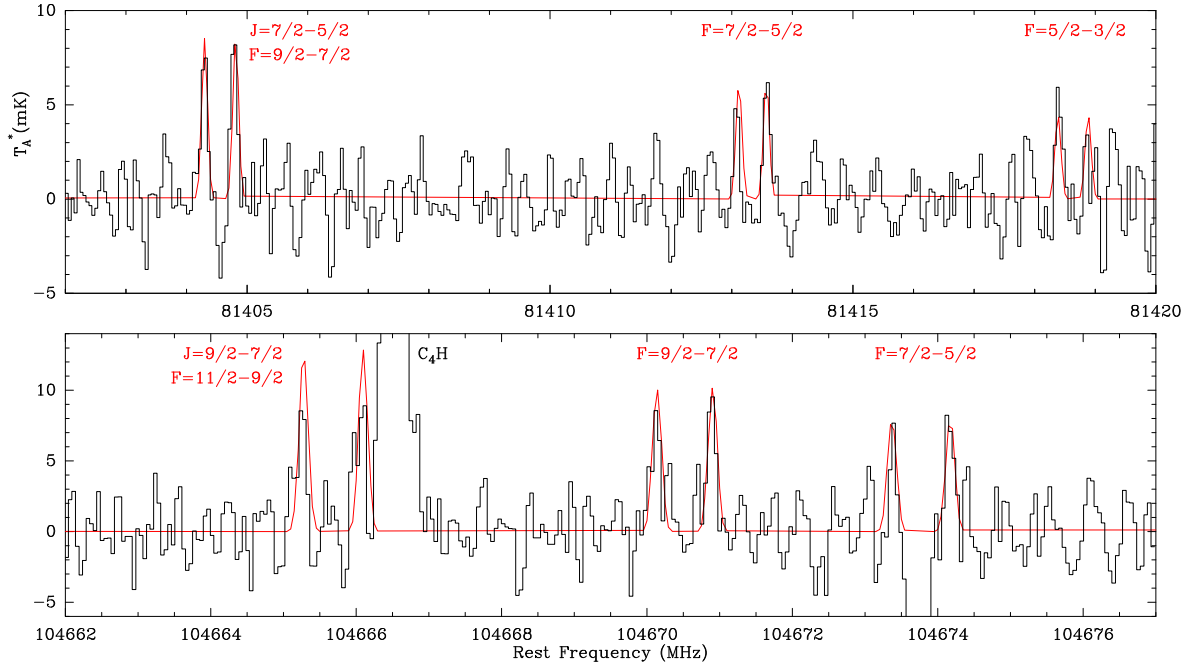

Fig. 1. Observed transitions of NCO in the $^2\Pi_{3/2}$ state towards L483. The strongest components of the $J = 7/2 - 5/2$ and $J = 9/2 - 7/2$ transitions are shown in the *upper* and *lower panels*, respectively. The LTE results are overplotted in red. We note that the absorption feature in the lower panel between the doublet $F = 7/2 - 5/2$ is not real, it is the corresponding negative of the C_4H line due to the frequency switching observing mode (located 7.2 MHz away).

The detection of NCO and H_2NCO^+ around a low-mass protostar such as L483 can thus shed light on the formation of prebiotic molecules containing the C(=O)–N group, such as HNCO and its isomers, or other species such as NH_2CHO and CH_3NCO (Cernicharo et al. 2016; Quénard et al. 2018).

2. Observations

The data presented here are part of a full 3 mm (80–116 GHz) spectral line survey of L483, using the IRAM 30 m radio telescope in Granada (Spain). The line survey observations were performed in several sessions in August and November 2016 and in May and December 2017. We also obtained Director's Discretionary Time to confirm the detection of NCO and H_2NCO^+ in January 2018. The observed position corresponds to that of the infrared source IRAS 18148–0440, that is $\alpha_{J2000} = 18^h17^m29.8^s$ and $\delta_{J2000} = -04°39'38.0''$ (Fuller & Myers 1993).

We used the EMIR receivers operating at 3 mm, connected to the fast Fourier transform spectrometers (FTS) in high resolution mode, providing a spectral resolution of 50 kHz, which corresponds to velocity resolutions of ~0.13–0.19 km s^{-1} in the range 80–116 GHz. Thanks to the versatility of the EMIR and FTS, we could observe four different bands per spectral set-up covering 4×1.8 GHz of bandwidth. All the observations were carried out in frequency switching mode, with a frequency throw of 7.2 MHz. The pointing and focus were checked every 1 and 3 hours, respectively. Pointing errors were always within 3″. The 30 m beam sizes at 3 mm are between 30″ and 21″. Weather conditions were different from one observing period to other, ranging from good winter conditions, with 2–5 mm of precipitable water vapour (pwv), to average summer conditions, with pwv≤10 mm. Concerning the data presented in this work, system temperatures range between 90 K and 120 K and the final rms noise is ~1–4 mK, depending on frequency. The spectra were calibrated in antenna temperature corrected for atmospheric attenuation and for antenna ohmic and spillover losses using the ATM package (Cernicharo 1985; Pardo et al. 2001). Data reduction and analysis were carried out using the CLASS program of the GILDAS software[1].

3. Results

During the analysis of the spectral survey data, we have found a number of unidentified lines. Among these there are several features at 81.4 GHz and 104.6 GHz, which are coincident with the strongest components of the $J = 7/2 - 5/2$ and $J = 9/2 - 7/2$ transitions of the NCO radical in the $^2\Pi_{3/2}$ state (see Fig. 1). The radical NCO is a linear triatomic molecule with a $^2\Pi_i$ electronic ground state, where the $^2\Pi_{1/2}$ spin-orbit state lies 137 K above the $^2\Pi_{3/2}$ state. The rotational levels are split by Λ doubling, leading to e and f parities, and are further split owing to the interaction with the nuclear spin of ^{14}N, leading to a hyperfine structure (Saito & Amano 1970; Kawaguchi et al. 1985; see also CDMS[2]; Müller et al. 2005, and MADEX[3]; Cernicharo 2012). As early as 1978, this radical was predicted to be abundant in dark clouds (Prasad & Huntress 1978), although until now NCO had not yet been detected in space probably because of its low dipole moment (0.64 D, Saito & Amano 1970). The complex rotational spectrum of NCO helps in assigning the lines. The strongest components of the $J = 7/2 - 5/2$ and $J = 9/2 - 7/2$ are detected in L483; there is no missing line and the centre frequencies and relative intensities are in very good agreement with the values obtained from laboratory. With the identification of 12 different transitions, the detection of NCO can be considered secure.

We have also detected six lines arising from H_2NCO^+, which is the lowest energy isomer of protonated isocyanic acid (see Fig. 2). This ion has a large dipole moment

[1] http://www.iram.fr/IRAMFR/GILDAS
[2] http://www.astro.uni-koeln.de/cdms/
[3] https://nanocosmos.iff.csic.es/?page_id=1619

Table 1. Column densities and fractional abundances derived.

Species	N (cm^{-2})	X/H_2	HNCO/X
NCO	2.2×10^{12}	7.3×10^{-11}	5.5
H_2NCO^+	3.0×10^{10}	1.0×10^{-12}	400
$HNCOH^+$	$<2.3 \times 10^{10}$	$<7.7 \times 10^{-13}$	>520
HNCO	1.2×10^{13}	4.1×10^{-10}	–
HOCN	1.5×10^{11}	5.0×10^{-12}	80
HCNO	7.3×10^{10}	2.4×10^{-12}	160
HONC	$<8.3 \times 10^{9}$	$<2.8 \times 10^{-13}$	>1450

(4.13 D, Lattanzi et al. 2012) and has been tentatively detected towards the molecular clouds in the Galactic centre Sgr B2(N) in absorption at 20 and 40 GHz by Gupta et al. (2013). H_2NCO^+ is a planar molecular ion with a C_{2v} symmetry, in which the two H nuclei are equivalent. Thus, the rotational levels are separated into ortho (K_a odd) and para (K_a even) states and have statistical weights of 3:1. Because of the ^{14}N nuclear spin, H_2NCO^+ also presents quadrupole hyperfine structure. However it is unresolved in the L483 spectra (see Fig. 2) and we do not take it into account in the analysis below. Although the lines of H_2NCO^+ in L483 are weak, where T_A^* is between 5 and 10 mK, all of these lines are detected above the 3σ level (rms noise levels are 1.2–2 mK). Furthermore, the fact that all the strongest transitions covered in the 3 mm band are detected and well centred at the systemic velocity of L483 ($V_{LSR} \sim 5.3$ km s^{-1}; Fuller & Myers 1993; Agúndez et al. 2008) supports the identification.

Table A.1 lists all the observed transitions, together with the line parameters derived from Gaussian fits. Rest frequencies and spectroscopic data were taken from the MADEX catalogue (Cernicharo 2012). We computed column densities assuming local thermodynamic equilibrium (LTE) and $T_{rot} = 10$ K, which is consistent with the values obtained for other species in this cloud (Agúndez et al. 2015a,b). For NCO, since the range of upper level energies covered by the observed transitions is narrow (6.6–11.7 K; see Table A.1), the rotational temperature is poorly constrained using rotational diagrams. In the case of H_2NCO^+, we have a relatively low number of transitions available when considering ortho and para species separately; in particular only two transitions are observed for the para state. Derived column densities are $N = (2.2 \pm 0.7) \times 10^{12}$ cm^{-2} for NCO, and 3.0×10^{10} cm^{-2} for H_2NCO^+ (values for the ortho and para species are $(2.1 \pm 0.5) \times 10^{10}$ cm^{-2} and $(8.6 \pm 3.9) \times 10^9$ cm^{-2}, respectively). In the line survey we also covered two transitions of HNCO, HOCN, and HCNO. We computed column densities for all these species assuming $T_{rot} = 10$ K. The fourth isomer, HONC, and the ion $HNCOH^+$ are not detected, and hence only upper limits are provided. The column densities and fractional abundances derived are listed for all species in Table 1. We used $N(H_2) = 3 \times 10^{22}$ cm^{-2}, which was derived by Tafalla et al. (2000) from observations of $C^{17}O$.

4. Discussion

The chemical processes linking H, C, O, and N atoms take place in combustion processes but the kinetics at the low temperatures of interstellar clouds is subject to many uncertainties. To investigate the formation of NCO and H_2NCO^+ in L483, we updated the chemical schema used in Marcelino et al. (2009); Marcelino et al. (2010) by considering the UMIST (McElroy et al. 2013) and KIDA (Wakelam et al. 2015) databases. In the absence of experimental or theoretical information on the kinetics, we verified the energy balance of various reactions. Table A.2 reports our estimate of the formation enthalpies of various isomers of the $CHNO^+$ and CH_2NO^+ ions, which are not all reported in thermodynamic tables nor in the KIDA database. We find that some reactions suggested in KIDA are in fact endothermic, for example

$$HOCN^+ + H_2 \rightarrow H_2OCN^+ + H, \quad (1)$$

$$HCNO^+ + H_2 \rightarrow H_2CNO^+ + H. \quad (2)$$

It is obvious that our tentative chemical network is subject to many uncertainties. Amongst these, the DR rate coefficients of the CH_2NO^+ ions and the branching ratios are critical. The

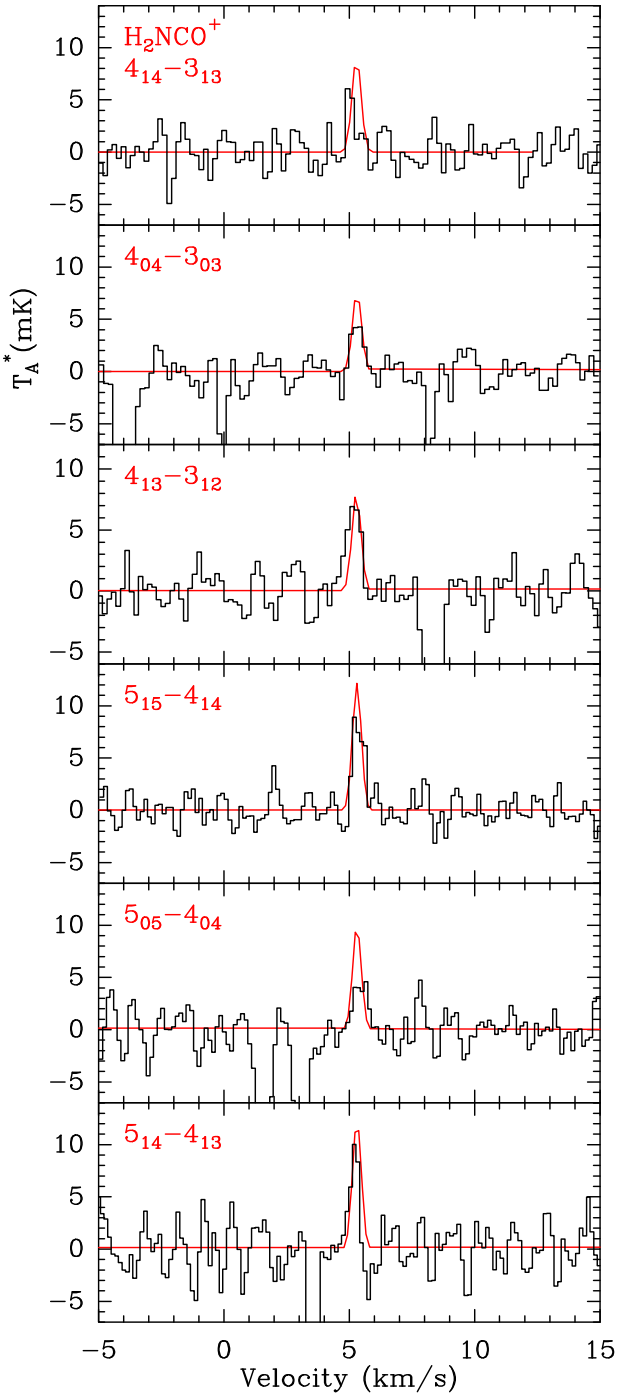

Fig. 2. Observed transitions of H_2NCO^+ towards L483. The LTE results are overplotted in red.

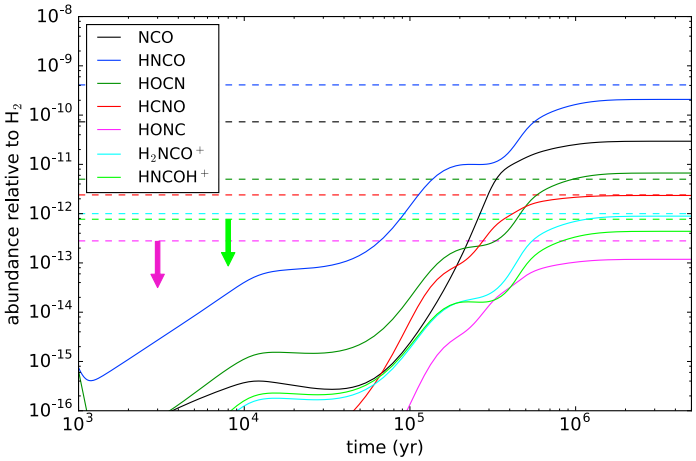

Fig. 3. Fractional abundances calculated as a function of time with our chemical model (see text). Horizontal dashed lines indicate the abundances derived from observations.

present model results are obtained when ejection of H and H_2 are favoured compared to other neutral channel products. In the cases in which two CHNO isomers are produced in the DR, we also assumed that the most stable is produced preferentially. The corresponding reaction rate coefficients are shown in Table A.3. Another uncertainty in our chemical network is the formation route of H_2NCO^+ through the NH_3 + HCO^+ reaction, which is exothermic. For this channel we assume a rate coefficient of $2.5\times10^{-10}(T/300)^{-0.5}$ cm^3 s^{-1}, while for the rapid proton transfer channel leading to NH_4^+ + CO we consider a higher rate coefficient of $2.2\times10^{-9}(T/300)^{-0.5}$ cm^3 s^{-1}.

In Fig. 3 we show the time evolution of the abundances of various species of interest, as given by our gas-phase chemical model. We adopt a H_2 volume density of 3.4×10^4 cm^{-3} and a gas kinetic temperature of 10 K, which are adequate for the L483 cloud (Fuller & Myers 1993; Anglada et al. 1997; Jørgensen et al. 2002). The cosmic ionization rate is fixed to 1.3×10^{-17} s^{-1} and the elemental abundances of C, N, O, and S relative to hydrogen are set to 9×10^{-6}, 1×10^{-5}, 1.5×10^{-5}, and 2×10^{-8}, respectively. The relative abundances for the detected species are rather well reproduced by our model, while those of HONC and $HNCOH^+$ are below the observed upper limits. Given the uncertainties of the chemical network, the agreement between the model and observations is very satisfactory.

The different species treated in this paper appear to follow different reaction routes, both through neutral-neutral reactions and ion-molecule schema. NCO is formed straightforwardly through the CN + O_2 reaction at a reaction rate of 2.4×10^{-11} cm^3 s^{-1} (Glarborg et al. 1998). Fulminic acid (HCNO), despite an energy of about 68 kcal mol^{-1} above the most stable isomer HNCO, is one of the main products, together with HCN, of the reaction between CH_2 and NO, as found in the laboratory (Grussdorf et al. 1994) and explained theoretically (Roggenbuck & Temps 1998). HNCO and HOCN, on the other hand, are rather formed through ion molecule schema as products in the DR of H_2NCO^+ and $HNCOH^+$, although the reaction for the latter has not yet been studied in the laboratory. The detection of H_2NCO^+ validates the occurrence of the ion-molecule formation schema.

5. Conclusions

In this letter we report the first detection in space of the NCO radical with a significant abundance of only ~5 times lower than HNCO towards the low-mass protostar L483. We have also detected H_2NCO^+ in this dense core, which together with NCO are involved in the production of HNCO and some of its isomers. We obtained similar abundances of HOCN and HCNO in L483, which is consistent with what was found by Marcelino et al. (2010) in dense cores. It is possible that NCO and H_2NCO^+ could be present in these sources as well. Unfortunately the corresponding frequencies were either not covered or the available data were not sensitive enough. Observations of NCO in sources at various stages across the star formation process could help to elucidate its role in the synthesis of CHNO isomers and prebiotic molecules containing the C(=O)–N group.

Acnowledgements. We thank the referee for his/her useful comments, and the IRAM 30 m staff for their help during the observations and time allocation of the DDT project. We acknowledge funding support from the European Research Council (ERC Grant 610256: NANOCOSMOS) and from Spanish MINECO through grant AYA2016-75066-C2-1-P. M.A. also acknowledges funding support from the Ramón y Cajal programme of Spanish MINECO (RyC-2014-16277). E.R. acknowledges partial support by the French programme "Physique et Chimie du Milieu Interstellaire" (PCMI) funded by the Conseil National de la Recherche Scientifique (CNRS) and Centre National d'Études Spatiales (CNES). M.T. acknowledges support from MINECO through grant AYA2016-79006-P.

References

Agúndez, M., Cernicharo, J., Guélin, M., et al. 2008, A&A, 478, L19
Agúndez, M., Cernicharo, J., & Guélin, M. 2015a, A&A, 577, L5
Agúndez, M., Cernicharo, J., de Vicente, P., et al. 2015b, A&A, 579, L10
Agúndez, M., Marcelino, N., Cernicharo, J., & Tafalla, M. 2018, A&A, 611, L1
Anglada, G., Sepúlveda, I., & Gómez, J. F. 1997, A&AS, 121, 255
Brünken, S., Belloche, A., Martín, S., Verheyen, L., & Menten, K. M. 2010, A&A, 516, A109
Cernicharo, J. 1985, Internal IRAM report (Granada: IRAM)
Cernicharo, J. 2012, in ECLA-2011: Proc. of the European Conference on Laboratory Astrophysics, EAS Pub. Ser., eds. C. Stehlé, C. Joblin, & L. d'Hendecourt (Cambridge: Cambridge Univ. Press)
Cernicharo, J., Kisiel, Z., Tercero, B., et al. 2016, A&A, 587, L4
Cernicharo, J., Lefloch, B., Agúndez, M., et al. 2018, A&A, 853, L22
Fuller, G. A., & Myers, P. C. 1993, ApJ, 418, 273
Glarborg, P., Alzueta, M. U., Dam-Johansen, K., & Miller, J. A. 1998, Combust. Flame, 115, 1
Grussdorf, J., Nolte, J., Temps, F., & Wagner, H. G. 1994, Ber. Bunsenges. Phys. Chem, 98, 546
Gupta, H., Gottlieb, C. A., Lattanzi, V., Pearson, J. C., & McCarthy, M. C. 2013, ApJ, 778, L1
Ijjaali, F., Alcami, M., Mó, O., & Yá nez M. 2001, Mol. Phys., 99, 1129
Jørgensen, J. K., Schöier, F. L. & van Dishoeck, E. F. 2002, A&AS, 389, 908
Kawaguchi, K., Saito, S., & Hirota, E. 1985, Mol. Phys., 55, 341
Lattanzi, V., Thorwirth, S., Gottlieb, C. A., & McCarthy, M. C. 2012, J. Phys. Chem. Lett., 3, 3420
Lias, S. G., Liebman, J. F., & Levin, R. D. 1984, J. Phys. Chem. Ref. Data, 13, 695
Loison, J.-C., Agúndez, M., Marcelino, N., et al. 2016, MNRAS, 456, 4101
Luna, A., Mebel, A. M., & Morokuma, K. 1996, J. Chem. Phys., 105, 3187
Marcelino, N., Cernicharo, J., Tercero, B., & Roueff, E. 2009, ApJ, 690, L27
Marcelino, N., Brünken, S., Cernicharo, J., et al. 2010, A&A, 516, A105
McElroy, D., Walsh, C., Markwick, A. J., et al. 2013, A&A, 550, A36
Müller, H. S. P., Schlöder, F., Stutzki, J., & Winnewisser, G. 2005, J. Mol. Struct. 742, 215
Oya, Y., Sakai, N., Watanabe, Y., et al. 2017, ApJ, 837, 174
Pardo, J. R., Cernicharo, J., & Serabyn, E. 2001, IEEE Trans. Antennas Propag., 49, 12
Park, Y.-S., Panis, J.-F., Ohashi, N., et al. 2000, ApJ, 542, 344
Prasad, S. S., & Huntress, Jr. W. T. 1978, MNRAS, 185, 741
Quan, D., Herbst, E., Osamura, Y., & Roueff, E. 2010, ApJ, 725, 2101
Quénard, D., Jiménez-Serra, I., Viti, S., Holdship, J., Coutens, A. 2018, MNRAS, 474, 2796
Roggenbuck, J., & Temps, F. 1998, Chem. Phys. Lett., 285, 422
Saito, S. & Amano, T. 1970, J. Mol. Spectr., 34, 383
Sakai, N., Sakai, T., Hirota, T., et al. 2009, ApJ, 697, 769
Schuurman M. S., Muir, S. R., Allen, W. D., & Shaefer III, H. F. 2004, J. Chem. Phys., 120, 11586
Tafalla, M., Myers, P. C., Mardones, D., & Bachiller, R. 2000, A&A, 359, 967
Wakelam, V., Loison, J.-C., Herbst, E., et al. 2015, ApJS, 217, 20

Appendix A: Additional tables

Table A.1. Observed transitions and line parameters derived from Gaussian fits.

Transition	Frequency (MHz)	E_{up} (K)	A_{ul} (s^{-1})	$\int T_A^* dv$ (mK km s^{-1})	V_{LSR} (km s^{-1})	Δv (km s^{-1})	T_A^* (mK)
NCO ($^2\Pi_{3/2}$)							
$J = 7/2 - 5/2$ $F = 9/2 - 7/2$ e	81404.300	6.6	$9.19\ 10^{-7}$	3.6(9)	5.32(4)	0.42(10)	8.0
$J = 7/2 - 5/2$ $F = 9/2 - 7/2$ f	81404.813	6.6	$9.19\ 10^{-7}$	4.1(9)	5.41(3)	0.42(7)	9.0
$J = 7/2 - 5/2$ $F = 7/2 - 5/2$ e	81413.120	6.6	$8.44\ 10^{-7}$	2.1(9)	5.45(4)	0.34(10)	5.9
$J = 7/2 - 5/2$ $F = 7/2 - 5/2$ f	81413.573	6.6	$8.44\ 10^{-7}$	3.2(9)	5.26(4)	0.45(10)	6.6
$J = 7/2 - 5/2$ $F = 5/2 - 3/2$ e	81418.385	6.6	$8.17\ 10^{-7}$	2.9(9)	5.24(6)	0.44(11)	6.2
$J = 7/2 - 5/2$ $F = 5/2 - 3/2$ f	81418.884	6.6	$8.17\ 10^{-7}$	1.6(9)	5.43(5)	0.27(17)	5.4
$J = 9/2 - 7/2$ $F = 11/2 - 9/2$ e	104665.278	11.7	$2.19\ 10^{-6}$	5.0(9)	5.45(5)	0.55(10)	8.6
$J = 9/2 - 7/2$ $F = 11/2 - 9/2$ f	104666.098	11.7	$2.19\ 10^{-6}$	5.4(9)	5.43(4)	0.55(7)	9.1
$J = 9/2 - 7/2$ $F = 9/2 - 7/2$ e	104670.139	11.7	$2.08\ 10^{-6}$	3.6(9)	5.36(4)	0.45(11)	7.6
$J = 9/2 - 7/2$ $F = 9/2 - 7/2$ f	104670.905	11.7	$2.08\ 10^{-6}$	3.9(9)	5.35(3)	0.37(8)	9.9
$J = 9/2 - 7/2$ $F = 7/2 - 5/2$ e	104673.371	11.7	$2.05\ 10^{-6}$	1.6(9)	5.26(4)	0.22(7)	7.1
$J = 9/2 - 7/2$ $F = 7/2 - 5/2$ f	104674.173	11.7	$2.05\ 10^{-6}$	2.9(9)	5.32(4)	0.35(8)	7.8
H_2NCO^+							
$4_{1,4} - 3_{1,3}$	80246.376	8.7	$4.28\ 10^{-5}$	2.0(5)	5.02(1)	0.18(60)	10.4
$4_{0,4} - 3_{0,3}$	80906.926	9.7	$4.67\ 10^{-5}$	2.8(5)	5.32(5)	0.53(9)	4.9
$4_{1,3} - 3_{1,2}$	81565.636	8.8	$4.49\ 10^{-5}$	4.9(9)	5.16(5)	0.63(10)	7.3
$5_{1,5} - 4_{1,4}$	100306.949	13.5	$8.74\ 10^{-5}$	5.0(5)	5.37(3)	0.53(5)	8.9
$5_{0,5} - 4_{0,4}$	101131.130	14.6	$9.33\ 10^{-5}$	3.8(9)	5.45(7)	0.70(15)	5.0
$5_{1,4} - 4_{1,3}$	101955.974	13.7	$9.18\ 10^{-5}$	4.2(9)	5.20(4)	0.38(8)	10.4
$HNCOH^+$							
$5 - 4$	99559.525	14.3	$8.82\ 10^{-6}$	<0.8			<3.3
HNCO							
$4_{0,4} - 3_{0,3}$ $F = 3 - 3$	87924.381	10.5	$7.25\ 10^{-7}$	19(1)	5.33(1)	0.33(2)	53.5
$4_{0,4} - 3_{0,3}$ $F = 5 - 4$	87925.252	10.5	$9.02\ 10^{-6}$	761(2)	5.31(1)	0.44(1)	1619.6
$4_{0,4} - 3_{0,3}$ $F = 4 - 3$	87925.252	10.5	$8.46\ 10^{-6}$				
$4_{0,4} - 3_{0,3}$ $F = 3 - 2$	87925.252	10.5	$8.29\ 10^{-6}$				
$4_{0,4} - 3_{0,3}$ $F = 4 - 4$	87925.898	10.5	$5.64\ 10^{-7}$	24(1)	5.30(1)	0.40(2)	57.4
$5_{0,5} - 4_{0,4}$ $F = 4 - 4$	109904.922	15.8	$8.81\ 10^{-7}$	12(1)	5.33(1)	0.34(3)	33.2
$5_{0,5} - 4_{0,4}$ $F = 6 - 5$	109905.758	15.8	$1.80\ 10^{-5}$	553(1)	5.31(1)	0.36(1)	1450.3
$5_{0,5} - 4_{0,4}$ $F = 5 - 4$	109905.758	15.8	$1.73\ 10^{-5}$				
$5_{0,5} - 4_{0,4}$ $F = 4 - 3$	109905.758	15.8	$1.71\ 10^{-5}$				
$5_{0,5} - 4_{0,4}$ $F = 5 - 5$	109906.430	15.8	$7.21\ 10^{-7}$	11(1)	5.31(2)	0.37(4)	28.2
HOCN							
$4_{0,4} - 3_{0,3}$	83900.569	10.1	$4.18\ 10^{-5}$	50(1)	5.31(1)	0.47(1)	99.7
$5_{0,5} - 4_{0,4}$	104874.676	15.1	$8.36\ 10^{-5}$	34(1)	5.30(1)	0.38(1)	83.2
HCNO							
$4 - 3$	91751.320	11.0	$3.84\ 10^{-5}$	21(1)	5.33(1)	0.41(2)	47.4
$5 - 4$	114688.383	16.5	$7.67\ 10^{-5}$	8(2)	5.35(3)	0.26(5)	28.6
HONC							
$4 - 3$	87625.193	10.5	$3.41\ 10^{-5}$	<2.1			<8.1
$5 - 4$	109530.044	15.8	$6.81\ 10^{-5}$	<1.6			<6.9

Notes. Rest frequencies and spectroscopic data are taken from the MADEX catalogue (Cernicharo 2012).

Table A.2. Formation enthalpy estimates in kcal mol^{-1}.

Species	ΔH	Ref.
$HNCO^+$	243	1
$HOCN^+$	274	2
$HCNO^+$	292	2
$HONC^+$	331.7	2
$HNOC^+$	331.4	2
H_2NCO^+	167	1
$HNCOH^+$	183	3
$HCNOH^+$	234.8	3
H_2OCN^+	240.9	3
H_2CNO^+	243	3

Notes. (1) Lias et al. (1984); (2) computed from Luna et al. (1996) using the experimental value for the most stable isomer $HNCO^+$; (3) computed from Ijjaali et al. (2001) using the experimental value for the most stable isomer H_2NCO^+.

Table A.3. Assumed rate coefficients of the DR reaction of the CH_2NO^+ ions.

Reaction	Rate coefficient ($\times 10^{-7}$(T/300)$^{-0.5}$ cm^3 s^{-1})
$H_2NCO^+ + e \rightarrow HNCO + H$	2.50
$H_2NCO^+ + e \rightarrow CO + NH_2$	0.50
$H_2NCO^+ + e \rightarrow NCO + H_2$	1.50
$H_2CNO^+ + e \rightarrow HCNO + H$	2.50
$H_2CNO^+ + e \rightarrow CH_2 + NO$	0.50
$HCNOH^+ + e \rightarrow HCNO + H$	2.50
$HCNOH^+ + e \rightarrow HONC + H$	0.50
$HCNOH^+ + e \rightarrow HCN + OH$	0.50
$HNCOH^+ + e \rightarrow HOCN + H$	0.50
$HNCOH^+ + e \rightarrow HNCO + H$	2.50
$HNCOH^+ + e \rightarrow HNC + OH$	0.50
$H_2OCN^+ + e \rightarrow HOCN + H$	1.50
$H_2OCN^+ + e \rightarrow H_2O + CN$	0.50